HHS Public Access

Author manuscript

Hepatology. Author manuscript; available in PMC 2018 May 01.

Published in final edited form as:

Hepatology. 2017 May ; 65(5): 1526–1542. doi:10.1002/hep.29021.

TM6SF2 rs58542926 impacts lipid processing in liver and small intestine

Elizabeth A. O'Hare[a,*], **Rongze Yang**[a,*], **Laura Yerges-Armstrong**[a], **Urmilla Sreenivasan**[a], **Rebecca McFarland**[a], **Carmen C. Leitch**[a], **Meredith H. Wilson**[c], **Shilpa Narina**[a], **Alexis Gorden**[a,b], **Kathy Ryan**[a], **Alan R. Shuldiner**[a], **Steve A. Farber**[c], **G. Craig Wood**[d], **Christopher D. Still**[e], **Glenn S. Gerhard**[d,e], **Janet D. Robishaw**[d], **Carole Sztalryd**[a,f,**], and **Norann A. Zaghloul**[a,**]

[a]Division of Endocrinology, Diabetes and Nutrition, Department of Medicine, University of Maryland School of Medicine, Baltimore, MD 21201, USA

[c]Carnegie Institution for Science, Department of Embryology, Baltimore, MD 21218, USA

[d]Geisinger Clinic, Geisinger Obesity Research Institute, Danville PA 17822, USA

[f]Baltimore VA Medical Center, VA Research Service, Geriatric Research, Education and Clinical Center (GRECC) and VA Maryland Health Care System, 10N Green Street Baltimore 21201, USA

Abstract

The transmembrane 6 superfamily member 2 (*TM6SF2*) loss-of-function variant, rs58542926, is a genetic risk factor for nonalcoholic fatty liver disease and progression to fibrosis, but is paradoxically associated with lower levels of hepatic-derived triglyceride-rich lipoproteins (TRLs). *TM6SF2* is expressed predominately in liver and small intestine, sites for triglyceride rich lipoprotein biogenesis and export. In light of this, we hypothesized that TM6SF2 may exhibit analogous effects on both liver and intestine lipid homeostasis. To test this, we genotyped rs58542926 in 983 bariatric surgery patients from the Geisinger Medical Center for Nutrition and Weight Management, Geisinger Health System (GHS) in PA and from 3,556 study participants enrolled in the Amish Complex Disease Research Program (ACDRP). Although these two cohorts have different metabolic profiles, carriers in both cohorts had improved fasting lipid profiles. Importantly, following a high fat challenge, carriers in the ACDRP cohort exhibited significantly lower postprandial serum triglycerides suggestive of a role for TM6SF2 in the small intestine. To gain further insight into this putative role, effects of TM6SF2 deficiency were studied in a zebrafish model and in cultured human Caco-2 enterocytes. In both systems TM6SF2-deficiency resulted in defects in small intestine metabolism in response to dietary lipids including significantly increased lipid accumulation, decreased lipid clearance and increased endoplasmic

[**]Authors for Correspondence: Norann A. Zaghloul, 660 W. Redwood Street, Howard Hall 487, Baltimore, MD 21201, Phone: 410-706-1646, Fax: 410-706-1622, zaghloul@umaryland.edu. Carole Sztalryd, 660 W. Redwood Street, Howard Hall 445A, Baltimore, MD 21201, Phone: 410-706-4047, Fax: 410-706-1622, cztalry@grecc.umaryland.edu.

[b]Current affiliation: Mid Atlantic Permanente group, Largo, MD 20774, USA

[e]Current affiliation: Department of Medical Genetics and Biochemistry, Temple University School of Medicine, Philadelphia, PA 19140, USA

[*]These Authors Contributed Equally

reticulum stress. *Conclusions:* These data strongly support a role of TM6SF2 in regulation of postprandial lipemia potentially through a similar function for TM6SF2 in the lipidation and/or export of both hepatically- and intestinally-derived TRLs.

Keywords

triglyceride-rich lipoproteins; missense mutation; endoplasmic reticulum stress; cytosolic lipid droplets; non-alcoholic fatty liver disease

Non-alcoholic fatty liver disease (NAFLD) is highly prevalent among obese and insulin resistant individuals who are also at risk of developing elevated circulating lipids and cardiovascular disease (CVD) (1, 2). Recently, however, a paradoxical increased susceptibility to NAFLD with low circulating lipids was found in carriers of a loss of function variant, rs58542926, in the transmembrane 6 super family member 2 gene (*TM6SF2*) (3–5). Given that dyslipidemia is a major contributor to atherosclerosis and CVD (6–8), this paradox offers the potential to define mechanisms by which hepatic steatosis can be dissociated from increased CVD risk factors. Understanding the biological function of TM6SF2 may offer critical insight into the etiology of both pathologies.

The *TM6SF2* rs58542926 variant is a cytosine to thymine substitution at coding nucleotide 499, resulting in a glutamate to lysine substitution at residue 167 (E167K). While overproduction of apolipoprotein B (apoB)-containing lipoproteins by the liver and intestine is one hallmark of obesity-associated NAFLD and an independent risk factor of CVD, carriers of *TM6SF2* E167K have increased liver lipid stores and unexpectedly lower serum triglyceride (TG), lower low-density lipoprotein-cholesterol (LDL-C), and total cholesterol. They also appear protected from CVD despite a higher risk of non-alcoholic steatohepatitis (NASH) (3–5, 9–13). TM6SF2 is localized mainly in the endoplasmic reticulum (ER) membrane and is predominantly expressed in liver and small intestine, two organs involved in packaging and secretion of dietary lipids in TG-rich lipoproteins (TRL) and regulation of whole body lipid homeostasis (3). Previous mechanistic studies focused primarily on the impact of *TM6SF2* loss-of-function in liver. These reports confirmed the loss-of-function nature of the E167K variant, demonstrating that it results in reduced levels of the protein compared to wild type *TM6SF2* in cultured hepatocytes (3). Moreover, knockdown of *Tm6sf2* in mice with short hairpin RNA (shRNA) increased liver TG content and decreased very low density lipoprotein (VLDL) secretion, offering a hepatic mechanism underlying co-occurrence of NAFLD and reduced circulating lipids (3). The role of intestinal *TM6SF2*, however, remains unexplored.

The major objective of this study was to investigate whether *TM6SF2* may impact intestinal lipid homeostasis similar to its role in liver. Specifically, we tested the hypothesis that TM6SF2 loss-of-function results in increased lipid accumulation and decreased lipid secretion in the small intestine. Given the association of E167K in humans with NAFLD and progression to NASH (3, 11, 13–15), we also characterized potential subcellular mechanisms by which TM6SF2 loss-of-function contributes to both. We evaluated TM6SF2 loss-of-function on ER stress due to ER localization of the endogenous protein (5) and the crucial role of ER stress in development of steatosis and progression to NASH (16). We

performed association studies for lipid traits in the Geisinger Health system (GHS) bariatric surgery and in the Amish Complex Disease Research Program (ACDRP) cohorts followed by *in vivo* and *in vitro* mechanistic studies in zebrafish and cultured human enterocytes, respectively. Our findings confirmed the association of E167K with NAFLD and NASH in the GHS cohort and with improved lipid profiles in the GHS and ACDRP cohorts despite wide differences in energy homeostasis status between these two cohorts. Upon further examination of the association of circulating lipids with *TM6SF2* loss-of-function in the ACDRP cohort we found evidence for reduced fasting and postprandial lipemia after a high fat challenge, suggesting a role for TM6SF2 in regulating intestinal postprandial lipid homeostasis. We then modeled TM6SF2 loss-of-function *in vivo* using larval zebrafish, an optically transparent model useful for whole animal studies of lipid metabolism (17, 18) and cultured human Caco-2 enterocytes (19). Our results indicated that loss of TM6SF2 function leads to lipid accumulation in enterocytes, similar to hepatocytes, as well as a similar increase in ER stress in both tissues. Together, these findings suggest that TM6SF2 regulates both hepatic and intestinal lipid and ER homeostasis,.

Experimental Procedures

Study Participants

The *TM6SF2* rs58542926 variant was genotyped in 983 bariatric surgery patients in the GHS cohort and 3556 participants in the ACDRP cohort. Tests of association were carried out for effect of E167K on serum lipids, liver histology (GHS cohort only) and hepatic fat content by electron-beam computerized tomography (EBCT; ACDRP cohort only). A high fat feeding intervention was performed in the ACDRP cohort to evaluate effect of E167K on fasting and post-challenge lipid traits (20). Institutional review board approval was obtained from the Geisinger Clinic and University of Maryland and all subjects provided written informed consent.

Zebrafish Experiments—Zebrafish embryos were microinjected with morpholino antisense (control, *tm6sf2,* or *dgat2*) alone or with human *TM6SF2* RNA. Larvae were assessed for morpholino efficacy, gene expression, LDL-C levels, hepatic steatosis via oil red O staining, and ER dilation and cytosolic lipid droplet (CLD) number and size via transmission electron microscopy (TEM) in liver and intestine. Zebrafish care and experimental procedures were carried out in accordance with the Animal Care and Use Committees of the University of Maryland.

Cell culture experiments—Caco-2 cells from ATCC (Manassas, VA) were treated with lentiviral short hairpin RNA (shRNA) targeting *TM6SF2* and assessed for CLD accumulation by BODIPY staining and confocal imaging analysis (21). TG synthesis and secretion were determined by [3H]oleic acid pulse chase experiments (22) and [3H]oleic acid incorporated into TG or secreted into culture media as previously described (21).

All experimental details and statistical analyses are provided in the online supplemental material

Results

Association of TM6SF2 rs58542926 with improved fasting and postprandial lipid profiles in humans

We first examined the relevance of TM6SF2 function to NAFLD in a large bariatric surgery cohort at the Geisinger Medical Center (Danville, PA) (total N=983) (Supplemental Table 1). Individuals with at least one copy of the rs58542926 variant (T*M6SF2*; c. *C>T*; p. Glu>Lys; N=130) exhibited a higher average steatosis grade of 1.40±0.08 versus 1.14±0.03 in non-carriers (N=853; p=0.04; Supplemental Table 2). In addition, 43.8% of T allele carriers exhibited lobular inflammation versus 32.4% carrying the major allele (p=0.02; Supplemental Table 2). Consistent with previous reports (12, 13), rs58542926 was associated with perivenular fibrosis in 26.6% of carriers versus 17.5% of non-carriers (p=0.008; Supplemental Table 2). These data suggest that rs58542926 is associated with increased liver steatosis and increased risk for progression to NASH in extreme obesity. Despite the dyslipidemia typically associated with obesity, fasting lipid levels, total cholesterol, TG and LDL-C were also lower in carriers of the T allele and statistically significant only in the subgroup also exhibiting NAFLD (p=0.02 for total cholesterol and p=0.004 for TG; Supplemental Table 1 and Table 3).

The rs58542926 minor allele frequency (MAF=6.7%) in the GHS bariatric surgery cohort translated to a small number of homozygous participants (n=3), hindering our ability to assess the impact of carrying two copies of the T allele for this variant. To address this, we analyzed a large founder population cohort from the ACDRP (N=3556), inclusive of non-obese subjects, in which the rs58542926 T allele is significantly enriched (MAF=12%) compared to outbred European populations and thus resulting in a larger number of homozygotes (n=51; 1.4%). Association analysis of carriers in the ACDRP cohort revealed: i) no association to BMI, fasting glucose or insulin, steatosis or alanine transaminase (ALT) (steatosis: $\beta=0.03\pm0.09$, p=0.68; ALT: $\beta=0.005\pm0.016$, p=0.75), ii) lower alkaline phosphatase (ALKP) ($\beta=-0.03\pm0.01$, p=0.003), iii) lower TG, total cholesterol and LDL-C ($p<7.1\times10^{-6}$, $p<3.6\times10^{-6}$; and $p<2.1\times10^{-8}$, respectively), and iv) higher high density lipoprotein cholesterol (HDL-C), ($p<5.0\times10^{5}$) (Supplemental Tables 4 and 5).. Lipid sub-fraction data from a subset of participants (n=833) indicated that rs58542926 carriers had lower total non-HDL-C ($p=2.7\times10^{-9}$), very low density lipoprotein (VLDL-C; $p=2.4\times10^{-4}$), $VLDL_3$-C ($p=2.2\times10^{-4}$), intermediate density lipoprotein (IDL-C; $p=1.9\times10^{-6}$), real LDL-C ($p=3.5\times10^{-8}$) and remnant lipoprotein-C ($p=9.8\times10^{-6}$), but not HDL or HDL-related sub-fractions (p>0.09; Supplemental Table 6). Lipid profiles of 807 genotyped individuals from the ACDRP cohort who underwent high-fat challenge were available for analysis (20) (Figure 1). T allele carriers of rs58542926 exhibited lower postprandial triglyceridaemia ($p<9.9\times10^{-3}$) with lower total area under the curve ($\beta=-9.5$, p<0.005) and incremental area under the curve ($\beta=-4.25$, p<0.02; Figure 1). Moreover, apoB48 levels measured at 2 hours post-meal were significantly lower in the rs58542926 T allele homozygotes (19.1±7.5 vs 13.1±6.0, values are ± SEM, n=12, p<0.02 adjusted for age and sex) This suggests a substantial delay in appearance of ingested lipid into circulating TG and impaired lipid

processing by the small intestine. These data therefore prompted us to pursue mechanistic studies in a zebrafish model of *TM6SF2* loss-of-function.

Modeling *TM6SF2* loss of function in zebrafish

The rs58542926 variant is a loss-of-function allele (3–5), To model its function, we carried out genetic knockdown in a model organism, the zebrafish, in which hepatic and intestinal lipid homeostasis could be easily observed. We first verified that *tm6sf2* was expressed in larval zebrafish liver and gut by wholemount *in situ* hybridization and qRT-PCR (Supplemental Fig 1A–B). Expression continued to be abundant in liver and intestine at adult stages (Supplemental Fig 1C). We then targeted endogenous expression of the zebrafish ortholog of *TM6SF2*, *tm6sf2,* by antisense morpholino oligonucleotide (MO) injected into one-cell embryos. Both splice-blocking MOs, targeting exon 3 (*tm6sf2_e3 MO*) or exon 4 (*tm6sf2_e4 MO*), suppressed *tm6sf2* expression, with *tm6sf2_e4* MO exhibiting more potency at earlier stages and lack of MO-related off-target effects as detected by no change in p53Δ113 gene expression, a pro-apoptotic gene isoform associated with MO off-target effects (Supplemental Figure 2A–C; (23)). We therefore used the *tm6sf2_e4* MO to model *tm6sf2* loss of function in all subsequent experiments. Suppression of *tm6sf2* through this approach increased the proportion of larvae exhibiting visible hepatic lipid ($p<1\times10^{-10}$; Figure 2B) versus control MO-injected larvae (Figure 2A,B), correlating with an increased number of CLDs quantified within a 49 nm^2 area of the liver. The average CLD number was 29.9±2.3 and 8.9±3.6 for exon 4 and control, respectively (values are ± SEM; n≥75; $p<1\times10^{-20}$; Figure 2B and Supplemental Figure 3). To further validate our model of hepatic steatosis induced by *tm6sf2* loss of function in the zebrafish model, we performed CRISPR/Cas9-mediated disruption of the zebrafish *tm6sf2* locus by co-injection of larvae with Cas9 mRNA and gRNA targeting either exon 3 or exon 4. An increase of hepatic steatosis was observed in both CRISPR mutant lines (Supplemental Figure 4A–C). The mismatch at the genomic locus was confirmed by T7 endonuclease assays and sequencing (24) (Supplemental Figure 4).

We quantified LDL-C in *tm6sf2*-depleted and control MO larvae after dissecting livers and measuring LDL-C in the remaining carcass (25). With a control diet, carcass LDL-C decreased by *tm6sf2* disruption: 0.17±0.09 versus 1.90±0.19 for *tm6sf2_e4 MO* and control MO, ($p<0.003$; Figure 2C). Taken together, these data validate the zebrafish model for study of TM6SF2 function and suggest a *tm6sf2* role in ApoB-TRL secretion since ApoB-TRL and LDL are directly interrelated.

We next assessed the relevance of rs58542926 to systemic lipid homeostasis in zebrafish by co-injection of *tm6sf2_e4 MO* with either wild type human *TM6SF2* RNA or E167K RNA. Addition of wild type *TM6SF2* RNA expression but not E167K RNA completely rescued steatosis (Figure 2A and B), supporting the loss-of-function nature of E167K (3, 5, 13). The average number of liver CLDs was 31.3±3.6 and 32.9±3.2 with MO alone or E167K RNA co-injection, respectively, and 9.2±1.5 with co-injection of MO and wild type RNA ($p<1\times10^{-24}$) which was not significantly different from control MO (values are ± SEM, n≥75, ns).

tm6sf2 disruption is associated with both ER stress and steatosis

ER stress contributes to hepatic steatosis and progression to NASH (16). We therefore performed zebrafish studies to evaluate whether loss of *tm6sf2* also results in ER stress. TEM examination of liver ultrastructure in unfed 5 dpf larvae (Figure 3A) revealed an increase in CLDs in hepatocytes with *tm6sf2* knockdown versus control MO, consistent with hepatic CLD accumulation observed by whole mount oil red O staining (Figures 2A and B, 3A and B). Average CLD area/cell was 1825±238 versus 2878±325 with *tm6sf2_e4 MO* versus control MO, respectively ($p<0.005$; values are ± SEM, n=12 larvae and 31 cells) (Figure 3B). Knockdown of *tm6sf2* but not control MO resulted in ER cisternae dilation (supplemental Figure 6A and B): cisternae width was 63.7±7.3 nm versus 30.0±4.4 nm with *tm6sf2_e4 MO* versus control MO, respectively ($p\leq 3\times 10^{-64}$; values are ± SEM, n>100 ER cisternae). Markers of ER stress, including *chop, bip*, *edem1* and spliced *xbp1,* examined by qRT-PCR at 5 dpf, were also significantly increased in *tm6sf2* morphants versus controls (Figure 3C).

Similar results were obtained in human liver biopsies from rs58542926 carriers from the bariatric surgery cohort from the Geisinger Health System (Danville, PA). We examined the expression of ER stress markers including *CHOP*, *HSPA5*, *ATF6*, *ATF4* and spliced *XBP1* by qRT-PCR and found a significant increase in carriers of the variant compared to non-carriers with comparable degree of steatosis ($p<0.05$, $p<0.01$, $p<0.001$, and $p<0.05$, respectively). Increased ER was present irrespective of fibrosis (Figure 3D).

Together, these observations indicate that steatosis and ER stress are concurrently associated with TM6SF2 loss of function in both zebrafish and human livers (Figure 3A–D and supplemental Figure 6) warranting further investigation,

tm6sf2 is sufficient to rescue *foie-gras* mutant steatosis and ER stress

Given that over expression of *TM6SF2* mRNA reduced the proportion of wild type larvae exhibiting accumulation of hepatic lipid (Figure 2A and B), its over expression should also ameliorate lipid accumulation in a zebrafish model of NAFLD caused by ER stress. To test this possibility, we examined the *foie gras* (*foigr*) zebrafish mutant, which exhibits hepatic steatosis as a result of ER stress (26, 27). We injected progeny of heterozygous *foigr* carriers with RNA encoding wild type *TM6SF2*. Relative to untreated mutant larvae at 5 dpf, over expression of *TM6SF2* resulted in a significant decrease in the proportion of animals exhibiting oil red O staining in the liver (16% in *tm6sf2_e4 MO* larvae vs 23% in control MO larvae; Figure 4A and Supplemental Figure 4). Expression of the ER stress marker genes, *chop* and *edem1*, was also significantly reduced in livers of wild type *TM6SF2* RNA-injected larvae, relative to untreated control mutants (Figure 4B). In contrast, over expression of E167K into *foigr* larvae did not rescue hepatic steatosis as 85% of larvae displayed steatosis and produced an upregulation of all assessed genes associated with induction of ER stress (Figures 4A and 4B, Supplemental Figure 4).

tm6sf2 knockdown enhances tunicamycin-induced ER stress gene expression

To further explore the role of *tm6sf2* knockdown in ER stress, we examined whether pharmacological induction of ER stress phenocopies the *tm6sf2* knockdown ER stress

phenotype in zebrafish liver. We used tunicamycin (Tm), an antibiotic that blocks protein N-linked glycosylation in ER by inhibiting the transfer of GlcNAc to dolichol phosphate and typically causes full activation of most UPR target genes (26, 28, 29). To examine the possibility of an epistatic relationship between *tm6sf2* and ER stress, we used a combination of *tm6sf2* MO and tunicamycin treatment (30). Combining MO mediated knockdown of *tm6sf2* and Tm treatment enhanced ER stress gene expression (Supplemental Figure 7). However, TM6SF2 over expression did not rescue Tm induced ER stress (Supplemental Figure 7), suggesting that the mechanism by which *tm6sf2* deficiency disrupts ER homeostasis likely differs from the one underlying Tm induced ER stress.

Reduced TG synthesis ameliorates *tm6sf2* depletion-induced phenotypes

To determine if *tm6sf2*-induced ER stress could be alleviated by reduced production of TG, the major component of hepatic CLD, we examined the consequences of reducing TG production on the steatosis and ER stress phenotypes in zebrafish larvae lacking *tm6sf2*. We reduced TG formation by inhibiting Acyl-CoA: diacylglycerol acyltransferase 2 (*dgat2*), a key enzyme for the final step of TG biosynthesis that is highly expressed in liver (31). *dgat-2* MO treatment resulted in effective *dgat-2* gene knockdown at day 5.(Supplemental Figure 2). Knockdown of *dgat2* reduced *tm6sf2* knockdown-induced hepatic steatosis, as indicated by oil red O staining, to a level comparable to MO control treated larvae (Figure 5A). 89% of larvae injected with *tm6sf2_e4 MO* exhibited liver oil red O staining, a significant increase compared to control MO-treated larvae (25%) or larvae injected with both *tm6sf2* and *dgat2* (21%; Figure 5B). In addition, *dgat2* inhibition ameliorated *tm6sf2* depletion-induced ER stress. Elevated levels of expression for ER stress markers *chop*, *bip* and *edem1* by *tm6sf2* deletion were ameliorated by loss of *dgat2* (Figure 5C). These findings suggest that inhibition of TG synthesis reduced both hepatic steatosis and ER stress resulting from loss of *tm6sf2*.

Disruption of *tm6sf2* perturbs intestinal clearance of dietary lipid

TM6SF2 expression is highest in small intestine, in both humans and mice (Supplemental Figure 5A–B) and delayed postprandial TG excursion was observed in human E167K carriers, suggesting TM6SF2 has a role in intestinal lipid homeostasis similar to that in liver (Figure 1). To test this possibility, we assessed CLD content of enterocytes in zebrafish at 5 dpf, when larvae begin to rely on dietary lipid, by comparing histology and intestinal CLD in ultrathin section TEM of larval anterior intestine in three fed states: 1) unfed, 2) immediately after a high fat meal (3 hour HFD), 3) 18 hour after the 3 hour HFD, and 4) 24 hour after the 3 hour HFD. Unfed control larvae did not exhibit CLD accumulation in enterocytes (Figure 6A), but the average CLD area per cell surface area was about 30 fold greater in unfed *tm6sf2_e4 MO* larvae. ER cisternae dilation was also increased (Figure 6A–D), consistent with a *tm6sf2* role in enterocyte ER and lipid homeostasis in the absence of dietary lipid similar to its role in liver (Figure 3A–C and Supplemental Figure 6A and B). After a 3 hour HFD, CLDs increased in control larvae and then reduced following 18 hour clearance. The area of CLD relative to cell surface area was 1059±261.21 nm^2 after the 3 hour HFD and then reduced to 96.53±52.94 nm^2 after 18 hour clearance (values are ± SEM, n=4–12 larvae, $p<0.01$; Figure 7C). With *tm6sf2* depletion, an increase in CLD was also observed after 3 hour HFD (unfed 781.78±388.4 nm^2 vs 3 hour HFD 3221.4±681.62 nm^2,

values are ± SEM, n=12 larvae, p<0.001 (Figures 6A and 7A–C). However, the CLD accumulation observed in *tm6sf2* deficiency enterocytes after 3hr HFD was significantly greater than the CLD accumulation in control MO enterocytes (Figure 7A–D). Importantly, by 18hr after a 3hr HFD, while 90% of the accumulated fat was cleared in enterocytes from zebrafish treated with control MO, only 40% of accumulated fat was cleared in enterocytes from zebrafish treated with tm6sf2 MO.. By 24hr, there was no longer a statistical difference observed among the groups for total CLD area although *tm6sf2*-deficient enterocytes still contained a greater number of CLDs compare to control enterocytes (control 4.2±0.95 vs *tm6sf2* MO 12.9±2.6 average CLD/cell; values are ± SEM, n=12 larvae, p<0.001) (Figure 7C–D). Together with our human postprandial lipid measurement, these data support a likely role of TM6SF2 in small intestine lipid clearance.

TM6SF2 modulates lipid content in human Caco-2 enterocytes and is associated with ER stress

To assess whether our observations in zebrafish could be extrapolated to human cells, we transduced human Caco-2 enterocytes with lentiviral shRNA targeting *TM6SF2* (sh*TM6SF2*), resulting in 98% reduction of mRNA versus a scrambled shRNA control treatment (Figure 8A). Visualization of intracellular lipid by BODIPY 493/503 staining (21) indicated that *TM6SF2* depletion increased intracellular lipid content by 3.7 fold relative to control shRNA-treatment (p<0.01; 7–9 independent experiments; Figure 8A–B) in Caco-2 cells incubated with oleic acid (600μM for 16 hours) but not without exogenous oleic acid (data not shown), suggesting that *TM6SF2* depletion increases CLD in enterocytes in response to exogenous lipids. Further, examination of TG synthesis and secretion in enterocytes by pulse-chase studies with [(3)H]oleate indicated that *TM6SF2* depletion did not alter incorporation of exogenous oleate into intracellular TG, measured after 16 hours, but reduced incorporation into TG secreted into the media after a 1 hour "chase" (p<0.01; 3–4 independent experiments; Figure 8 C–D). Finally, we confirmed the ER localization of TM6SF2 in Caco-2 cells and upon treatment of *TM6SF2* shRNA-treated cells with oleic acid (600μM for 16 hours) we observed significantly increased expression of ER stress markers, including *HSPA5*, *ATF6*, *ATF4*, and *CHOP* compared to control (p<0.001, p<0.05, p<0.05, and p<0.01, respectively; Figure 8E and Supplemental Figure 4D). These results corroborate our observations in zebrafish and strongly support a TM6SF2 role in processing of dietary lipids in human enterocytes.

Discussion

Our findings indicate that *TM6SF2* plays a role in both liver and enterocyte lipid homeostasis. Upon depletion of *TM6SF2* gene expression in human Caco-2 enterocytes, or its homolog in zebrafish, we observed significant lipid accumulation in response to exogenous lipid in either tissue. These observations are consistent with observations in human carriers of a TM6SF2 loss-of-function variant, which exhibit hepatic steatosis and ER stress progressing to fibrosis and inflammation along with significant decreases in fasting circulating lipids but also reduced postprandial triglyceride excursion. Our findings also reveal that increased ER stress as a result of loss of *TM6SF2* expression is concurrent with the observed increase accumulation of CLDs in both human and zebrafish tissues. The

rescue of both phenotypes from depletion of *TM6SF2* gene expression by simply blocking production of TG, and the observation of epistatic interaction with Tm. provide strong evidence that the *TM6SF2* gene function involves lipid homeostasis, which has a downstream impact on ER stress. Taken together, these findings suggest an important role for *TM6SF2* in mediation of circulating TG through a previously unidentified intestinal function that likely parallels its functions in liver. There is convincing evidence that hypertriglyceridemic states are associated with accelerated atherosclerosis and CVD (8, 32). Most TG is transported in the plasma by TRL that are either hepatically-derived VLDL or intestinally-derived chylomicrons, with considerable overlap of molecular players and pathways involved in processing across the repertoire of TRLs. Our data provide strong support for a role of *TM6SF2* in TRL processing, in both liver and intestine tissues.

In fasting conditions, TG is predominately carried in VLDL particles, whereas in the postprandial state TG is additionally carried in chylomicrons and their remnants (8). The role of *TM6SF2* in modulating VLDL secretion from liver is well documented and has been proposed as the primary mechanism by which fasting lipoprotein profiles are improved in carriers of the loss-of-function variant (3, 5). Importantly relevant to its function, ApoB-associated lipoproteins are primarily affected in carriers of the loss-of-function variant, as evidenced by the highly significant effects on LDL-C, VLDL-C, IDL-C, and TG. Our findings offer an additional mechanism by which *TM6SF2* depletion may contribute to improved CVD profile through its role in regulating postprandial intestine-derived TRLs. Our observation that TM6SF2 carriers of the T-allele have lower postprandial triglyceridaemia in response to a high fat challenge is in agreement with a recent published report (33). Although about 80% of the increase in circulating TG after a fat-load meal comes from apoB48-containing lipoproteins (34), approximately 80% of the increase in particle number is accounted for by VLDL particles (35, 36). ApoB48- and apoB100-containing particles are cleared from the circulation by common pathways and therefore compete for clearance (37). Our data support the need to further detailed human kinetic studies to understand the full impact of TM6SF2 in processing of apoB-lipoproteins, and relative contribution of liver and small intestine to the improved lipid profile.

The improved lipid profile in carriers of the E167K variant is in apparent conflict with the variant's adverse effects on NAFLD and progression to NASH. This suggests that impaired TRL secretion may be directly relevant to retention of intracellular lipid in hepatocytes. Intriguingly, we observed improved lipid profiles in carriers of the variant from two cohorts with vastly different metabolic profiles. The Old Order Amish (OOA) is a relatively healthy population with less diabetes, more physical activity and less alcohol consumption than the general population. The variant in *TM6SF2* was strongly correlated with reduced circulating lipids in the OOA, even in the absence of NAFLD or liver dysfunction (42, 43). In contrast, the variant was associated with increased steatosis, fibrosis and inflammation in the metabolically stressed conditions found in extremely obese bariatric surgery patients. Similarly, increased association with NASH was reported in obese children carrying the rs58542926 variant (10). These observations suggest a role for TM6SF2 in both liver and intestinal response, but perhaps underscore the role of metabolic stress in unmasking its deleterious effects in liver. Importantly, these findings support the possibility of a common intracellular mechanism by which TM6SF2 functions across tissues.

This suggests that the strength of the association of *TM6SF2* T allele with NAFLD and NAFLD progression may depend on additional factors that compromise hepatic lipid homeostasis. Indeed, our observations of increased association with steatosis, fibrosis, and inflammation in bariatric surgery patients might indicate that extreme obesity is a metabolic stress that impacts the presence of NASH associated with rs58542926. Similarly increased association with NASH was reported in obese children (10). This may be clinically relevant as it may indicate that interventions aiming at either reducing hepatic lipid flux or increasing lipid utilization may help circumvent the deleterious health consequences of the *TM6SF2* variant on liver lipid homeostasis. Overall, our observations in two cohorts with vastly different metabolic profiles support a role for TM6SF2 in both liver and intestinal response to dietary lipid with improved systemic lipid homeostasis. These data potentially support the possibility of a unifying mechanism at the level of TM6SF2 intracellular function.

Dietary fat absorption is a multistep process that involves temporary storage of dietary fat in CLDs of enterocytes and hepatocytes, and re-packaging in lipoprotein particles for transport (38). It is accepted that both CLDs and apoB-rich lipoproteins both originate within the ER bilayer from newly synthesized esterified lipids, but they mature on opposite sides of the bilayer (38). The current model of chylomicrons and VLDL assembly proposes a two-step process. In the first step newly synthesized apoB is lipidated during translocation across the ER into the lumen, yielding a primordial particle. In the second step, bulk transfer of core lipids is believed to take place postranslationally, involving lumenal LDs (39). Several lines of evidence support a role of TM6SF2 in the packaging and secretion of esterified lipids. Previous reports have indicated that TM6SF2 localizes to the ER in hepatocytes, consistent with our observations in enterocytes (5). In addition, our zebrafish and cell culture studies indicate that TM6SF2 deficiency reduced the flux of TG toward export in both tissues, and consequently CLD number is concurrently increased.

Our data also suggest that it is unlikely that processes upstream of the ER are impaired. It is not likely that fatty acid uptake is impaired given that the introduction of dietary lipid resulted in a significant increase in enterocyte lipid content. The absence of an uptake defect suggests that the localization of a defect is limited to an ER-localized defect in lipid packaging and synthesis or to post-ER trafficking and secretion.

The role of perturbations in the ER in NAFLD has become a subject of considerable interest in recent years (16). Notably, depletion of *tm6sf2* in zebrafish hepatocytes and enterocytes led to both increased CLD accumulation and ER stress in our zebrafish and human studies. Both of these phenotypes can be successfully rescued simply by *dgat2* knockdown, an indication that TG biogenesis and the *tm6sf2* loss associated lipid homeostasis phenotype might be causative of ER stress. Nonetheless, *TM6SF2* rescued both steatosis and ER stress in a zebrafish mutant, *foigr*, where steatosis is thought to be secondary to ER stress (26). *foigr* is highly conserved; T*RAPPC11* is the human ortholog, but its function remains elusive. Published data suggest that TRAPPC11 functions in the anterograde secretory pathway at an early stage in ER-to Golgi transport (40). In addition to its trafficking function, recent published data suggests that TRAPPC11 may also act upstream of the dolichyl-phosphate N-acetylglucosaminephosphotransferase (DPAGT1-CDC), the target enzyme responsible for Tm induced ER stress (41). However, results from our epistasis

experiments suggest that TM6SF2 over expression does not rescue Tm induced ER protein homeostasis, an indication that Tm and *tm6sf2* depletion activate ER stress by different mechanisms. If *TRAPPC11* deletion causes a backup of VLDL in the smooth ER (26), our data suggest that *TM6SF2* overexpression can compensate for the interrupted trafficking. VLDL and chylomicron precursors are assembled in the ER and their maturation occurs in the post-ER compartments (42). However, how this maturation is achieved is only partially understood. Our data support the novel hypothesis that TM6SF2 may be key to the process involved in ApoB lipoprotein maturation.

Further examination of the intracellular mechanisms underlying lipid accumulation will be necessary to fully clarify the function of TM6SF2 in hepatic and intestinal lipid accumulation. The identification of an important role of a single gene in both tissues which are central to regulation of systemic lipemia offers the exciting possibility of a single gene target to address elevated circulating TRLs from both sources. Further study will also potentially shed light onto other interactors that may collaborate with TM6SF2, revealing important insight into the regulation of TRL regulation and secretion. The elucidation of an intestinal role for TM6SF2 offers a first step towards such understanding.

Supplementary Material

Refer to Web version on PubMed Central for supplementary material.

Acknowledgments

Financial Support:

This research was supported by R01DK102001 (NAZ), T32AG000219 (EAO), RO1HL121007 (EAO), F32DK19592 (WIL), RODK1093399 (FAB), the Mid-Atlantic Nutrition Obesity Research Center (P30DK072488) and the Geriatric Research, Education and Clinical Center, Baltimore Veterans Affairs Health Care Center.

We thank Dr. Simeon Taylor for helpful discussion and guidance. We also thank our Amish liaisons and Amish Research Clinic staff, as well as the Amish community for cooperation and support and the patients and staff of the Geisinger Obesity Institute

List of Abbreviations

TM6SF2	transmembrane 6 superfamily member 2
TRLs	triglyceride-rich lipoproteins
ACDRP	Amish Complex Disease Research Program
NAFLD	Non-alcoholic fatty liver disease
CVD	Cardiovascular disease
E167K	Glutamate with lysine at residue 167
ApoB	apolipoprotein B
TG	triglyceride
LDL-C	low-density lipoprotein cholesterol

NASH	non-alcoholic steatohepatitis
ER	endoplasmic reticulum
shRNA	short hairpin RNA
VLDL	very low density lipoprotein
VLDL-C	very low density lipoprotein cholesterol
EBCT	electron-bean computerized tomography
RNA	ribonucleotide acid
CLD	cytosolic lipid droplet
TEM	transmission elctron microscopy
BMI	Body mass index
ALT	Alanine transaminase
ALKP	Alkaline phohatase
HDL-C	high density lipoprotein-cholesterol
IDL	Intermediate density lipoprotein
MO	Morpholino antisense
dpf	day post-fertilization
mRNA	messenger ribonucleic acid
gRNA	guide RNA
ApoB-TRL	apoB-triglyceride rich lipoprotein
LDL	Low density lipoprotein
SEM	Standard error of mean
ns	non significant
foigr	foie gras
DGAT2, Acyl-CoA	diacylglycerol acyltransferase 2
HFD	High fat meal
LDs	Lipid droplets
OOA	Older Order Amish

References

1. Choi SH, Ginsberg HN. Increased very low density lipoprotein (VLDL) secretion, hepatic steatosis, and insulin resistance. Trends Endocrinol Metab. 2011; 22:353–363. [PubMed: 21616678]
2. Tolman KG, Fonseca V, Dalpiaz A, Tan MH. Spectrum of liver disease in type 2 diabetes and management of patients with diabetes and liver disease. Diabetes Care. 2007; 30:734–743. [PubMed: 17327353]
3. Kozlitina J, Smagris E, Stender S, Nordestgaard BG, Zhou HH, Tybjaerg-Hansen A, Vogt TF, et al. Exome-wide association study identifies a TM6SF2 variant that confers susceptibility to nonalcoholic fatty liver disease. Nat Genet. 2014; 46:352–356. [PubMed: 24531328]
4. Holmen OL, Zhang H, Fan Y, Hovelson DH, Schmidt EM, Zhou W, Guo Y, et al. Systematic evaluation of coding variation identifies a candidate causal variant in TM6SF2 influencing total cholesterol and myocardial infarction risk. Nat Genet. 2014; 46:345–351. [PubMed: 24633158]
5. Mahdessian H, Taxiarchis A, Popov S, Silveira A, Franco-Cereceda A, Hamsten A, Eriksson P, et al. TM6SF2 is a regulator of liver fat metabolism influencing triglyceride secretion and hepatic lipid droplet content. Proc Natl Acad Sci U S A. 2014; 111:8913–8918. [PubMed: 24927523]
6. Taskinen MR, Boren J. New insights into the pathophysiology of dyslipidemia in type 2 diabetes. Atherosclerosis. 2015; 239:483–495. [PubMed: 25706066]
7. Nordestgaard BG, Varbo A. Triglycerides and cardiovascular disease. Lancet. 2014; 384:626–635. [PubMed: 25131982]
8. Chapman MJ, Ginsberg HN, Amarenco P, Andreotti F, Boren J, Catapano AL, Descamps OS, et al. Triglyceride-rich lipoproteins and high-density lipoprotein cholesterol in patients at high risk of cardiovascular disease: evidence and guidance for management. Eur Heart J. 2011; 32:1345–1361. [PubMed: 21531743]
9. Roh YS, Loomba R, Seki E. The TM6SF2 variants, novel genetic predictors for nonalcoholic steatohepatitis. Gastroenterology. 2015; 148:252–254.
10. Grandone A, Cozzolino D, Marzuillo P, Cirillo G, Di Sessa A, Ruggiero L, Di Palma MR, et al. TM6SF2 Glu167Lys polymorphism is associated with low levels of LDL-cholesterol and increased liver injury in obese children. Pediatr Obes. 2015
11. Dongiovanni P, Petta S, Maglio C, Fracanzani AL, Pipitone R, Mozzi E, Motta BM, et al. Transmembrane 6 superfamily member 2 gene variant disentangles nonalcoholic steatohepatitis from cardiovascular disease. Hepatology. 2015; 61:506–514. [PubMed: 25251399]
12. Daly AK, Day CP, Liu YL, Anstee QM. TM6SF2 as a genetic risk factor for fibrosis. Hepatology. 2015; 62:1321.
13. Liu YL, Reeves HL, Burt AD, Tiniakos D, McPherson S, Leathart JB, Allison ME, et al. TM6SF2 rs58542926 influences hepatic fibrosis progression in patients with non-alcoholic fatty liver disease. Nat Commun. 2014; 5:4309. [PubMed: 24978903]
14. Dongiovanni P, Romeo S, Valenti L. Genetic Factors in the Pathogenesis of Nonalcoholic Fatty Liver and Steatohepatitis. Biomed Res Int. 2015; 2015:460190. [PubMed: 26273621]
15. Sookoian S, Castano GO, Scian R, Mallardi P, Fernandez Gianotti T, Burgueno AL, San Martino J, et al. Genetic variation in transmembrane 6 superfamily member 2 and the risk of nonalcoholic fatty liver disease and histological disease severity. Hepatology. 2015; 61:515–525. [PubMed: 25302781]
16. Zhang XQ, Xu CF, Yu CH, Chen WX, Li YM. Role of endoplasmic reticulum stress in the pathogenesis of nonalcoholic fatty liver disease. World J Gastroenterol. 2014; 20:1768–1776. [PubMed: 24587654]
17. Schlegel A. Studying lipoprotein trafficking in zebrafish, the case of chylomicron retention disease. J Mol Med (Berl). 2015; 93:115–118. [PubMed: 25572701]
18. Schlegel A, Gut P. Metabolic insights from zebrafish genetics, physiology, and chemical biology. Cell Mol Life Sci. 2015; 72:2249–2260. [PubMed: 25556679]
19. Schlegel A. Studying non-alcoholic fatty liver disease with zebrafish: a confluence of optics, genetics, and physiology. Cell Mol Life Sci. 2012; 69:3953–3961. [PubMed: 22678663]

20. Pollin TI, Damcott CM, Shen H, Ott SH, Shelton J, Horenstein RB, Post W, et al. A null mutation in human APOC3 confers a favorable plasma lipid profile and apparent cardioprotection. Science. 2008; 322:1702–1705. [PubMed: 19074352]
21. Bell M, Wang H, Chen H, McLenithan JC, Gong DW, Yang RZ, Yu D, et al. Consequences of lipid droplet coat protein downregulation in liver cells: abnormal lipid droplet metabolism and induction of insulin resistance. Diabetes. 2008; 57:2037–2045. [PubMed: 18487449]
22. Caviglia JM, Sparks JD, Toraskar N, Brinker AM, Yin TC, Dixon JL, Brasaemle DL. ABHD5/CGI-58 facilitates the assembly and secretion of apolipoprotein B lipoproteins by McA RH7777 rat hepatoma cells. Biochim Biophys Acta. 2009; 1791:198–205. [PubMed: 19211039]
23. Robu ME, Larson JD, Nasevicius A, Beiraghi S, Brenner C, Farber SA, Ekker SC. p53 activation by knockdown technologies. PLoS Genet. 2007; 3:e78. [PubMed: 17530925]
24. Hwang WY, Fu Y, Reyon D, Maeder ML, Kaini P, Sander JD, Joung JK, et al. Heritable and precise zebrafish genome editing using a CRISPR-Cas system. PLoS One. 2013; 8:e68708. [PubMed: 23874735]
25. O'Hare EA, Wang X, Montasser ME, Chang YP, Mitchell BD, Zaghloul NA. Disruption of ldlr causes increased LDL-c and vascular lipid accumulation in a zebrafish model of hypercholesterolemia. J Lipid Res. 2014; 55:2242–2253. [PubMed: 25201834]
26. Cinaroglu A, Gao C, Imrie D, Sadler KC. Activating transcription factor 6 plays protective and pathological roles in steatosis due to endoplasmic reticulum stress in zebrafish. Hepatology. 2011; 54:495–508. [PubMed: 21538441]
27. Sadler KC, Amsterdam A, Soroka C, Boyer J, Hopkins N. A genetic screen in zebrafish identifies the mutants vps18, nf2 and foie gras as models of liver disease. Development. 2005; 132:3561–3572. [PubMed: 16000385]
28. Chen Z, Ballar P, Fu Y, Luo J, Du S, Fang S. The E3 ubiquitin ligase gp78 protects against ER stress in zebrafish liver. J Genet Genomics. 2014; 41:357–368. [PubMed: 25064675]
29. Lehle L, Tanner W. The specific site of tunicamycin inhibition in the formation of dolichol-bound N-acetylglucosamine derivatives. FEBS Lett. 1976; 72:167–170. [PubMed: 791682]
30. Levine AJ, Hu W, Feng Z, Gil G. Reconstructing signal transduction pathways: challenges and opportunities. Ann N Y Acad Sci. 2007; 1115:32–50. [PubMed: 17934060]
31. Yen CL, Stone SJ, Koliwad S, Harris C, Farese RV Jr. Thematic review series: glycerolipids. DGAT enzymes and triacylglycerol biosynthesis. J Lipid Res. 2008; 49:2283–2301. [PubMed: 18757836]
32. Miller M, Stone NJ, Ballantyne C, Bittner V, Criqui MH, Ginsberg HN, Goldberg AC, et al. Triglycerides and cardiovascular disease: a scientific statement from the American Heart Association. Circulation. 2011; 123:2292–2333. [PubMed: 21502576]
33. Musso G, Cassader M, Paschetta E, Gambino R. TM6SF2 may divert postprandial cholesterol toxicity away from the vessel walls to the liver in NAFLD. J Hepatol. 2015
34. Cohn JS, Johnson EJ, Millar JS, Cohn SD, Milne RW, Marcel YL, Russell RM, et al. Contribution of apoB-48 and apoB-100 triglyceride-rich lipoproteins (TRL) to postprandial increases in the plasma concentration of TRL triglycerides and retinyl esters. J Lipid Res. 1993; 34:2033–2040. [PubMed: 8301224]
35. Karpe F, Bell M, Bjorkegren J, Hamsten A. Quantification of postprandial triglyceride-rich lipoproteins in healthy men by retinyl ester labeling and simultaneous measurement of apolipoproteins B-48 and B-100. Arterioscler Thromb Vasc Biol. 1995; 15:199–207. [PubMed: 7749826]
36. Schneeman BO, Kotite L, Todd KM, Havel RJ. Relationships between the responses of triglyceride-rich lipoproteins in blood plasma containing apolipoproteins B-48 and B-100 to a fat-containing meal in normolipidemic humans. Proc Natl Acad Sci U S A. 1993; 90:2069–2073. [PubMed: 8446630]
37. Adiels M, Matikainen N, Westerbacka J, Soderlund S, Larsson T, Olofsson SO, Boren J, et al. Postprandial accumulation of chylomicrons and chylomicron remnants is determined by the clearance capacity. Atherosclerosis. 2012; 222:222–228. [PubMed: 22365426]
38. Sturley SL, Hussain MM. Lipid droplet formation on opposing sides of the endoplasmic reticulum. J Lipid Res. 2012; 53:1800–1810. [PubMed: 22701043]

39. Lehner R, Lian J, Quiroga AD. Lumenal lipid metabolism: implications for lipoprotein assembly. Arterioscler Thromb Vasc Biol. 2012; 32:1087–1093. [PubMed: 22517367]

40. Scrivens PJ, Noueihed B, Shahrzad N, Hul S, Brunet S, Sacher M. C4orf41 and TTC-15 are mammalian TRAPP components with a role at an early stage in ER-to-Golgi trafficking. Mol Biol Cell. 2011; 22:2083–2093. [PubMed: 21525244]

41. DeRossi C, Vacaru A, Rafiq R, Cinaroglu A, Imrie D, Nayar S, Baryshnikova A, et al. trappc11 is required for protein glycosylation in zebrafish and humans. Mol Biol Cell. 2016; 27:1220–1234. [PubMed: 26912795]

42. Sundaram M, Yao Z. Recent progress in understanding protein and lipid factors affecting hepatic VLDL assembly and secretion. Nutr Metab (Lond). 2010; 7:35. [PubMed: 20423497]

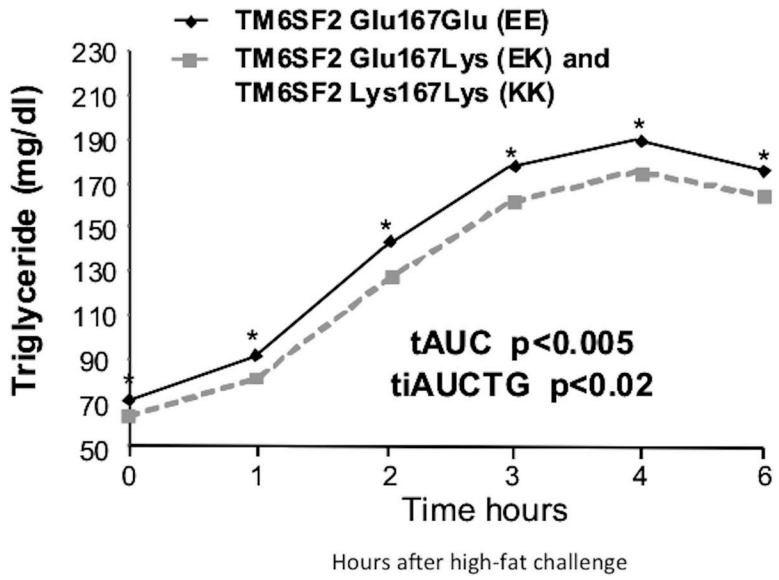

Figure 1.

T-allele carriers (EK and KK) have significantly reduced TG levels compared to their EE counterparts in response to a liquid meal: Triglycerides levels before and during the high fat challenge by E167K genotype. Shown are covariate-adjusted geometric means with 95% confidence intervals. Filled grey squares and hatched lines indicate individuals carrying the T allele and filled diamonds indicate non-carriers. Postprandial lipid responses were calculated as the AUC of the TG measurements at fasting, 1, 2, 3, 4 and 6 hours (p=0.05, p=0.03, p=0.008, p=0.04, p=0.05, p=0.05, respectively). The response relative to the baseline level was determined by calculating the incremental area under the curve (iAUC) of TG. The total area under the curve (AUC) of TG and postprandial TG levels and the incremental AUC (IAUC) were calculated and are shown in the insert with their respective p values.

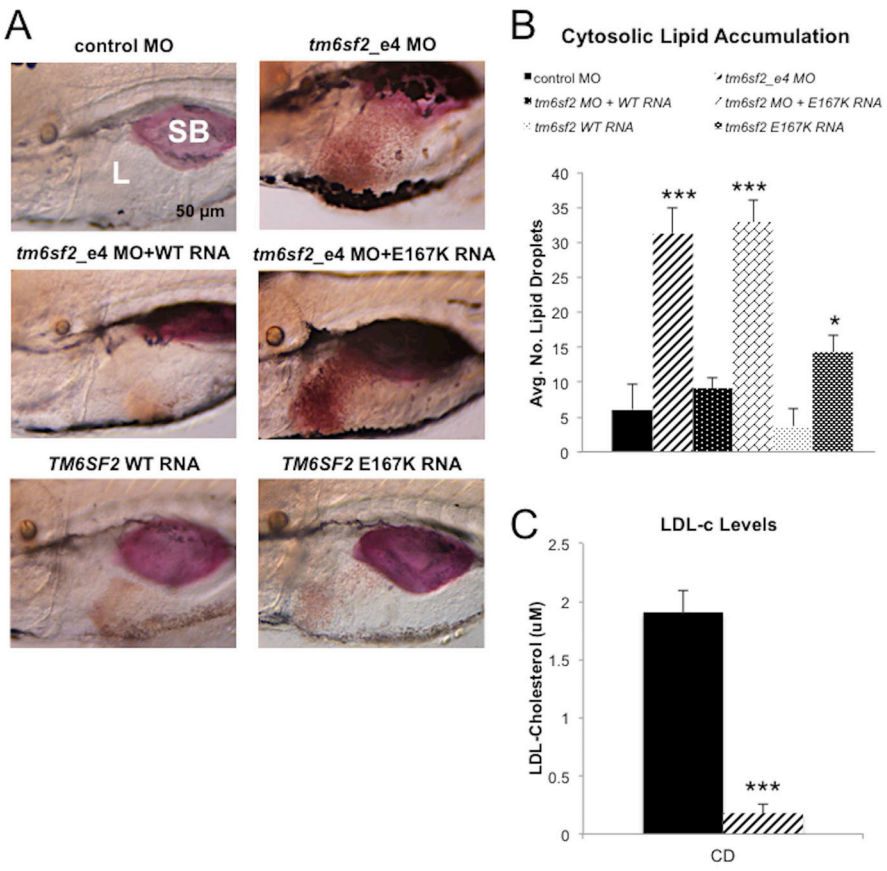

Figure 2. Loss of *tm6sf2* function in zebrafish results in hepatic lipid accumulation and reduced LDL-C

(A) Representative lateral view images of livers of Oil red O stained zebrafish larvae at 5 dpf. Shown from top left to bottom right: control MO, *tm6sf2_e4 MO*, co-injection of *tm6sf2_e4 MO* and wild type *TM6SF2* RNA, co-injection of *tm6sf2_e4 MO* with *TM6SF2* E167K mutant RNA, and injection of wild type *TM6SF2* RNA only. SB, swim bladder; L, liver. (B) Quantification of lipid accumulation shown as average number of lipid droplets per 49 nm^2 square area in livers of larvae treated as indicated (n=5). (C) LDL-C levels were quantified after removal of livers from control MO or *tm6sf2_e4 MO* larvae given a control diet for 48 hr starting at 5 dpf. Data represent average of triplicated values from 2 pooled groups of 100 larvae each per experiment for two separate experiments. *** $p \leq 1 \times 10^{-10}$.

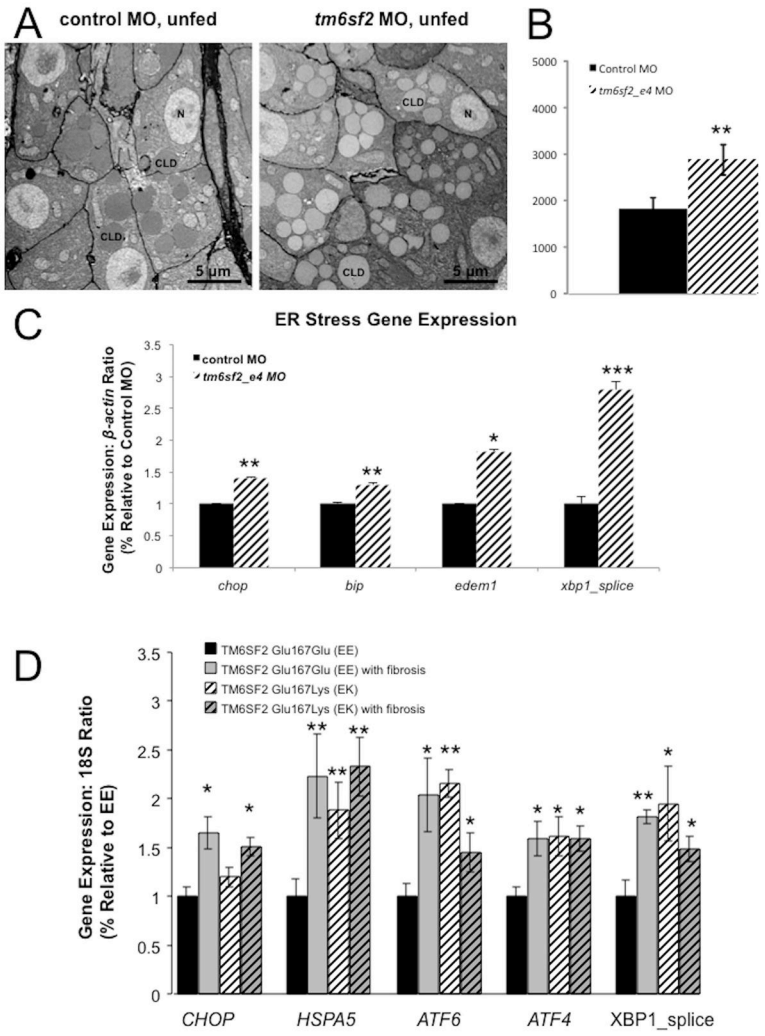

Figure 3. Increased hepatic lipid accumulation in *tm6sf2* morphants and ER stress. Similar increased expression of ER stress markers is observed in liver biopsies of TM6SF2 Glu167Lys (EK) carriers compared to TM6SF2 Glu167Glu (EE) counterparts

(A) Representative transmission electron microscopy (TEM) images of ultrathin 70 nm sections from livers of unfed control MO or *tm6sf2_e4 MO* larvae at 5 dpf assessed for hepatic lipid accumulation. CLD, cytosolic lipid droplet. (B) Quantification of hepatic lipid droplet accumulation shown as the average number of lipid droplets per nucleus. (C) Representative TEM images of ER cisternae (arrows) in livers of unfed control MO or *tm6sf2_e4* MO treated 5 dpf larvae. (D). qRT-PCR quantification of ER stress markers from 24 liver biopsies of TM6SF2 Glu167Glu (EE) and TM6SF2 Glu167Lys (EK) carriers. Six EE and EK carriers had been diagnosed with grade 0 or 1 steatosis but no fibrosis, 6 EE and EK with both steatosis (grade 1 and 2) and fibrosis. Patients were all female and morbidly obese. Results of triplicated assays, n = 6 each group, mean + SEM; *p<0.05, **p<0.01 for EE vs EE with fibrosis or EE vs EK or EE vs EK with fibrosis).

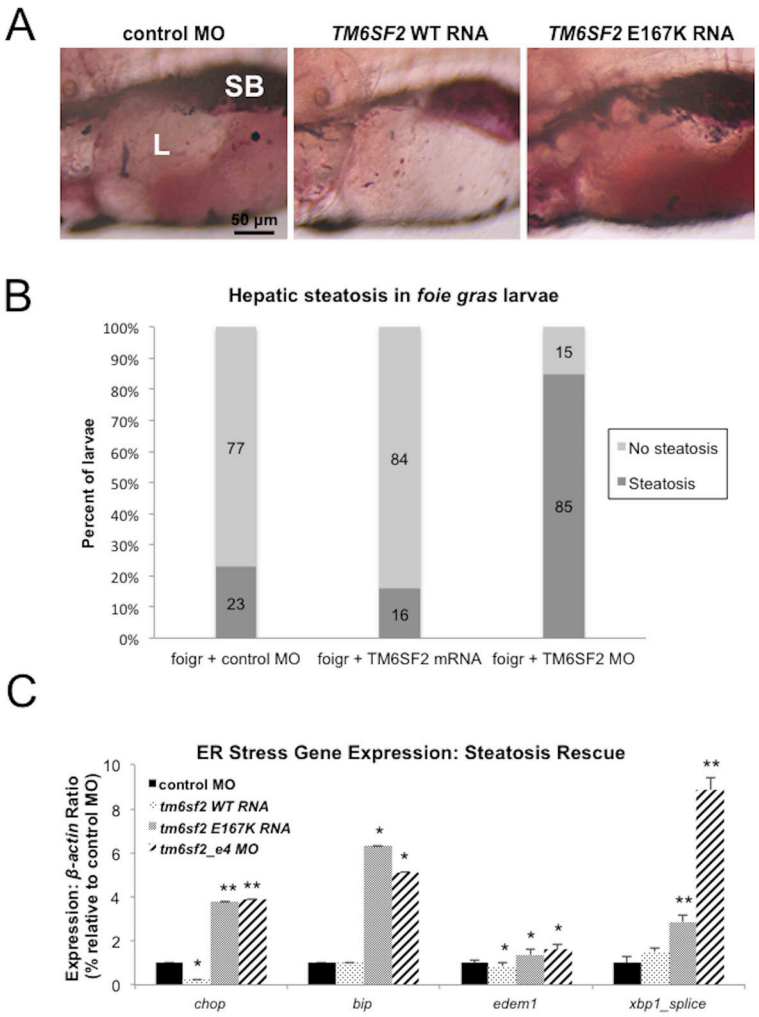

Figure 4. ER stress is ameliorated by *TM6SF2* wild-type overexpression in *foie gras* mutants

(A) Representative lateral view images of livers of oil red O stained *foigr* mutants injected with control MO, *TM6SF2* WT RNA, or *TM6SF2* E167K mutant RNA. SB, swim bladder; L, liver. (B) Quantification of gene expression by qRT-PCR for markers of ER stress in 5 dpf *foigr* larvae injected with either control MO, *TM6SF2* WT RNA, *TM6SF2* E167K mutant RNA or *tm6sf2_e4 MO*. Data represent average of triplicated values from 2 pooled groups of 40 larval livers each per experiment for two separate experiments. * $p<0.05$; ** $p<0.005$

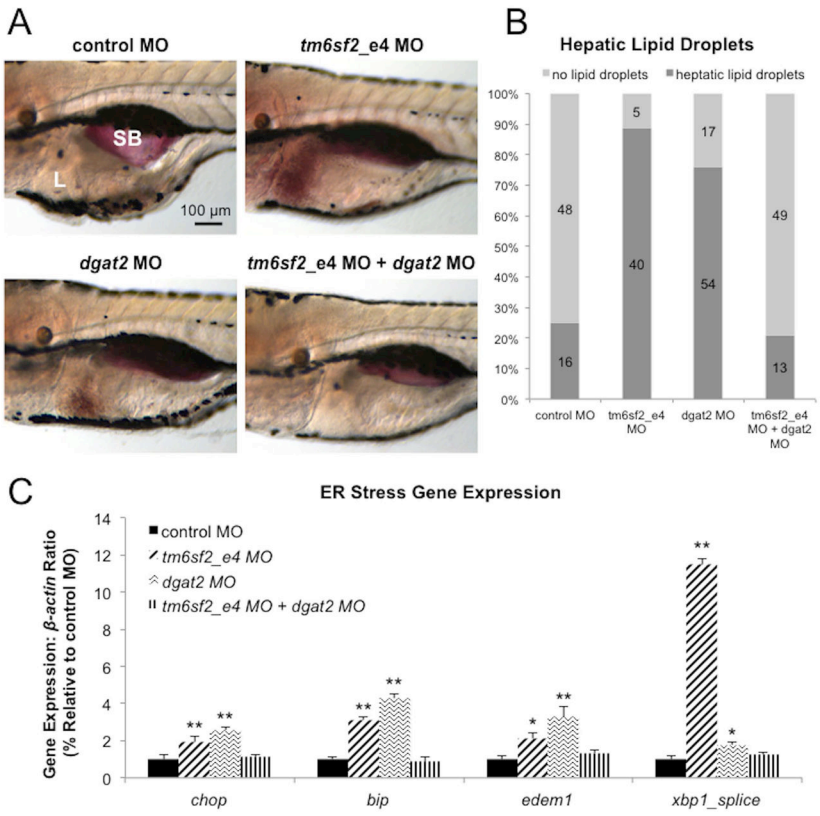

Figure 5. Inhibition of TG synthesis reduces hepatic steatosis and ER stress in *tm6sf2* morphants

(A) Representative lateral view images of livers from oil red O stained control larvae, larvae injected *tm6sf2_e4 MO* alone, or co-injected with *dgat2 MO*. SB, swim bladder; L, liver. (B) Quantification of the proportion of larvae exhibiting steatotic (dark grey) or normal livers (light grey). Numbers of total larvae used across two experiments shown on bars. (C) Quantification of ER stress marker gene expression by qRT-PCR from homogenized whole 5 dpf larvae injected control MO, *tm6sf2_e4 MO* alone, or *tm6sf2_e4 MO* and *dgat2 MO* together. Data represent average of triplicated values from 2 pooled groups of 20 larvae each per experiment for two separate experiments. ns: not significant; * $p<0.01$;** $p<0.0005$

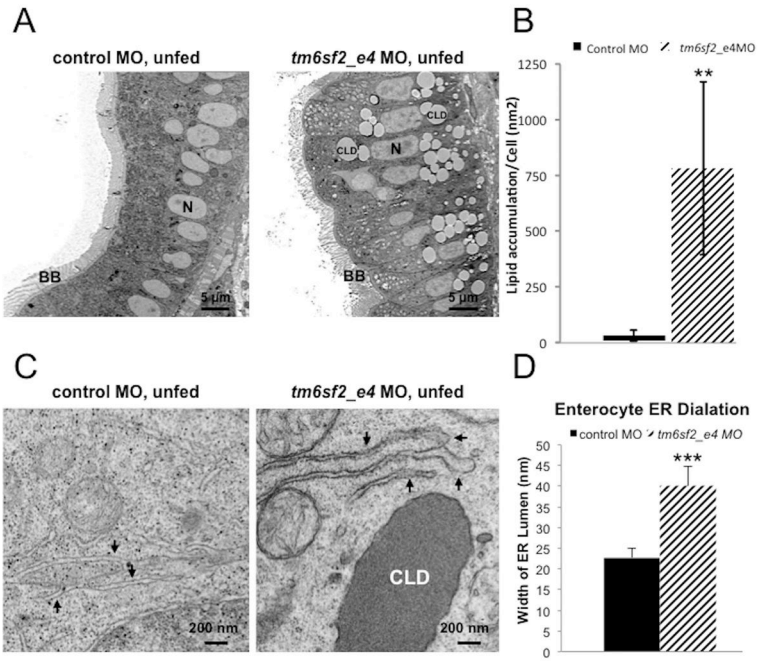

Figure 6. Depletion of *tm6sf2* results in lipid accumulation and ER stress in small intestine

(A) Representative TEM images of ultrathin 70 nm sections of enterocytes in anterior intestine from 5 dpf unfed control MO and *tm6sf2_e4 MO* larvae assessed for lipid accumulation. N, nucleus; BB, brush border; LD, lipid droplet. (B) Quantification of enterocyte lipid droplet accumulation in unfed control MO or *tm6sf2_e4 MO* larvae. Data calculated average lipid droplet area relative to total cell area measured in individual cells on images in which at least three contiguous cells with visible nuclei could be visualized. Data shown represent lipid droplet:cell size area as a proportion relative to control. n=12 larvae. (C) Representative TEM images of ER cisternae (arrows) from ultrathin 70 nm sections of enterocytes in anterior intestine. CLD, cytosolic lipid droplet. (D) Quantification of average ER lumen width measured from TEM images of larval intestine from unfed control MO or *tm6sf2_e4 MO* larvae. Data represent average width of 10 randomly selected smooth ER lumens per cell, three measurements per lumen. n=15 cells per treatment. ** $p<1\times10^{-10}$; ***$p<1\times10^{-10}$

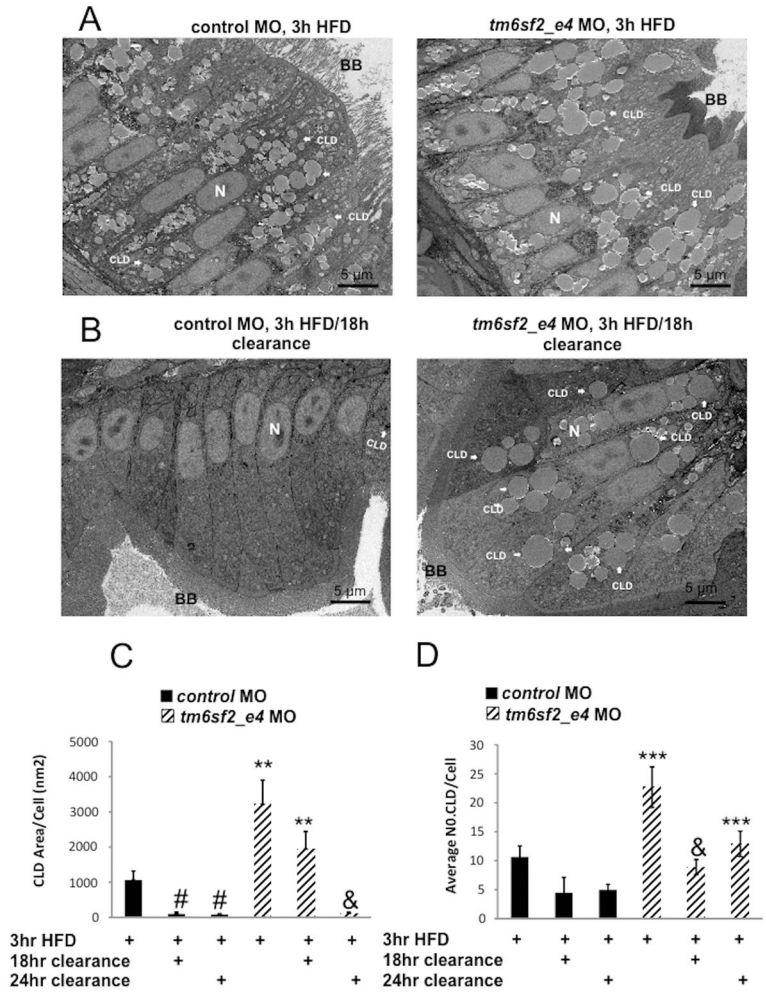

Figure 7. Loss of *tm6sf2* perturbs intestinal clearance of dietary lipid

Representative TEM images of ultrathin 70 nm sections from enterocytes in anterior intestine of larvae injected with control or *tm6sf2_e4 MO* treated with (A) high fat meal (HFD) for 3 hours or (B) a 3 hour HFD followed by 18 hour clearance. CLD, cytosolic lipid droplet. BB, brush border (C) Quantification of enterocyte CLD accumulation in control MO or *tm6sf2_e4 MO* larvae treated with a 3 hour HFD followed by 18- or 24-hour clearance. Data calculated average CLD area relative to total cell area measured in individual cells on images in which at least three contiguous cells with visible nuclei could be visualized, n=4–12 larvae. ** $p<0.01$ relative to control MO at same condition. # $p<0.01$ relative to control MO 3hr HFD; & $p<0.05$ relative to *tm6sf2* MO 3-hr HFD.. (D) Quantification of the number of enterocyte cytosolic lipid droplet per cell in control MO or *tm6sf2_e4 MO* larvae treated a 3 hour HFD followed by 18- or 24-hour clearance. n=4–12 larvae. *** $p<0.001$ relative to control MO at same condition. & $p<0.05$ relative to *tm6sf2* MO 3hr HFD.

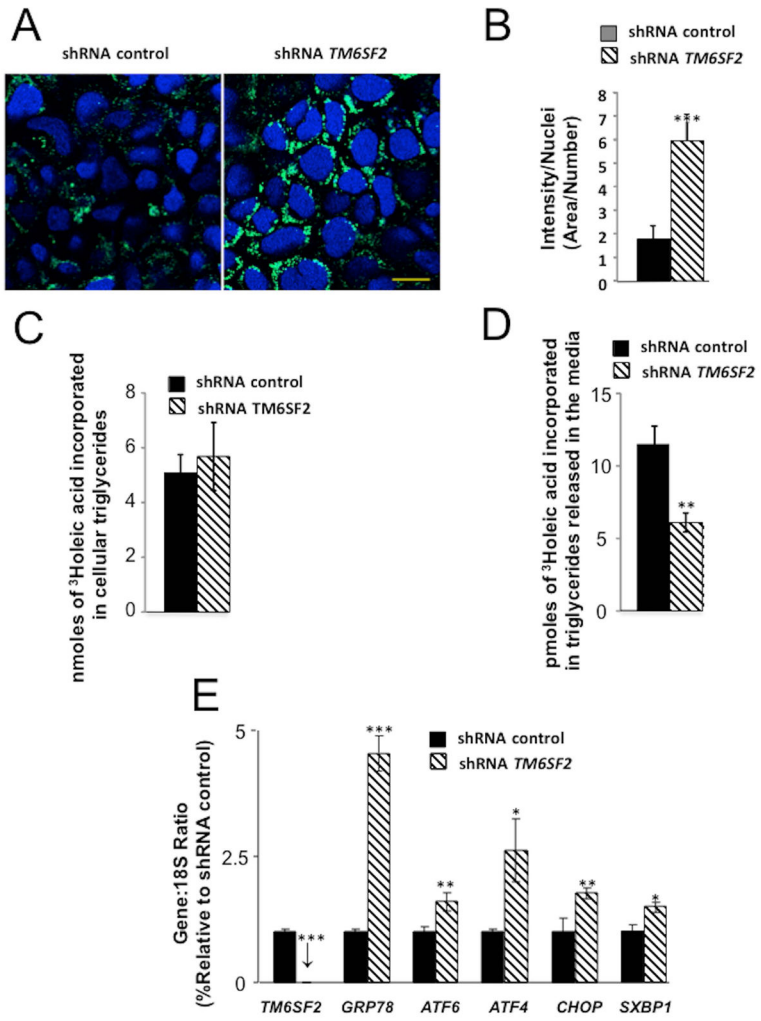

Figure 8. Effect of silencing TM6SF2 on cytosolic lipid droplet content of human Caco-2 cells, on TG synthesis and secretion and on ER stress gene expression

(A, B)Human Caco-2 cells were analyzed 48 hours after shRNA inhibition with *TM6SF2*-specific or control shRNA lentiviral vectors. Cells were incubated overnight with 400 μm oleic acid. The following day, cells were stained with DAPI and BODIPY493/503, fixed and analyzed by confocal microscopy. (A) Representative image (Scale bar, 10 μm). (B) Imaging analysis. Ratio of Bodipy fluorescence intensity to nuclei number normalized per area. Data are means±SE. from 7–9 independent experiments. ** $p<0.001$. (C, D) During the pulse period, cells were incubated for 16 hours in culture medium containing 0.6 mM [^{13}H]oleic acid complexed to fatty acid-free bovine serum albumin (BSA). Subsequently, during the washout period, the cells were incubated in culture medium containing 5 g fatty acid-free BSA per liter of medium for 1 hour. (C) Incorporated radioactivity in TG fraction of cells at the end of the pulse period. Data are mean±SE (n=3 independant experiments) (D) Incorporated radioactivity in TG fraction of media at the end of the 1hr washout, * $p<0.05$. Data are mean±SE(n=3 independent experiments) (E) Incubation of Caco-2 cells with OA (0.65 mM) for 16 h caused increased ER stress as evaluated by *GRP78*, *ATF6*, *ATF4*, *CHOP*

and spliced *XBP1* (*SXBP1*). *p<0.05, **p<0.01, ***p<0.01. Data are mean±SE (n=3 independent experiments).